Princeton Plasma Physics Laboratory

PPPL- 4482

PPPL- 4482

# Lithium Coatings on NSTX Plasma Facing Components and Its Effects On Boundary Control, Core Plasma Performance, and Operation

H.W. Kugel, M.G. Bell, H. Schneider, J.P. Allain, R.E. Bell, R Kaita, J. Kallman, S. Kaye, B.P.LeBlanc, D. Mansfield, R.E. Nygren, R.Maingi, J. Menard, D. Mueller, M.Ono, S.Paul, S. Gerhardt, R. Raman, S. Sabbagh, C.H. Skinner, V. Soukhanovskii, J.Timberlake, L.E. Zakharov, and the NSTX Research Team

January, 2010

PPPL PRINCETON PLASMA PHYSICS LABORATORY

Prepared for the U.S. Department of Energy under Contract DE-AC02-09CH11466.

# Princeton Plasma Physics Laboratory
# Report Disclaimers

---

## Full Legal Disclaimer



## Trademark Disclaimer



---

# PPPL Report Availability

## Princeton Plasma Physics Laboratory:

http://www.pppl.gov/techreports.cfm

## Office of Scientific and Technical Information (OSTI):

http://www.osti.gov/bridge

---

**Related Links:**

**U.S. Department of Energy**

**Office of Scientific and Technical Information**

**Fusion Links**

# Lithium Coatings on NSTX Plasma Facing Components and Its Effects On Boundary Control, Core Plasma Performance, and Operation

H.W.Kugel[1]*, M.G.Bell[1], H.Schneider[1], J.P.Allain[2], R.E.Bell[1], R Kaita[1], J.Kallman[1], S. Kaye[1], B.P.LeBlanc[1], D.Mansfield[1], R.E.Nygren[3], R.Maingi[4], J. Menard[1], D.Mueller[1], M.Ono[1], S.Paul[1], S.Gerhardt[1], R.Raman[5], S.Sabbagh[6], C.H.Skinner[1], V.Soukhanovskii[7], J.Timberlake[1], L.E.Zakharov[1], and the NSTX Research Team

[1] Princeton Plasma Physics Laboratory, PO Box 451, Princeton, NJ 08543, USA
[2] Purdue University, School of Nuclear Engineering, West Lafayette, IN 47907, USA
[3] Sandia National Laboratories, Albuquerque, NM 87185, USA
[4] Oak Ridge National Laboratory, Oak Ridge, TN 37831, USA
[5] University of Washington, Seattle, WA 98195, USA
[6] Columbia University, New York, NY 10027, USA
[7] Lawrence Livermore National Laboratory, Livermore, CA 94551, USA

NSTX high-power divertor plasma experiments have used in succession lithium pellet injection (LPI), evaporated lithium, and injected lithium powder to apply lithium coatings to graphite plasma facing components. In 2005, following wall conditioning and LPI, discharges exhibited edge density reduction and performance improvements. Since 2006, first one, and now two lithium evaporators have been used routinely to evaporate lithium onto the lower divertor region at total rates of 10-70 mg/min for periods 5-10 min between discharges. Prior to each discharge, the evaporators are withdrawn behind shutters. Significant improvements in the performance of NBI heated divertor discharges resulting from these lithium depositions were observed. These evaporators are now used for more than 80% of NSTX discharges. Initial work with injecting fine lithium powder into the edge of NBI heated deuterium discharges yielded comparable changes in performance. Several operational issues encountered with lithium wall conditions, and the special procedures needed for vessel entry are discussed. The next step in this work is installation of a Liquid Lithium Divertor surface on the outer part of the lower divertor.

**Keywords:** Lithium, lithium wall fusion regime, recycling, plasma wall interactions, divertors, spherical torus

## 1. Introduction

Density and impurity control, tritium and dust removal, and long-lifetime plasma facing components (PFCs) for diverted high power DT reactors are challenging technology problems. Replenishable liquid lithium PFCs show promise towards resolution of these challenges by providing a low-Z, pumping, self-healing plasma facing surface [1-3], and enabling a lithium wall fusion regime [4]. Preliminary work indicates that the use of liquid lithium as a PFC can help to integrate four important potential benefits for fusion, a) divertor pumping over large surface area compatible with high flux expansion solutions for power exhaust and low collisionality, b) improved confinement [5, 6], c) reduction or elimination of Edge Localized Modes (ELMs) [7-9], and d) high-heat flux handling [2, 10, 11].

### *1.1. National Spherical Torus Experiment lithium Research*

The National Spherical Torus Experiment (NSTX) [12, 13] has been investigating solid lithium (Li) coatings for density and impurity control [5-7]. In NSTX, recycling of deuterium species from plasma contact with ATJ graphite surfaces contributes to a secular density rise observed in most H-mode, neutral beam injection (NBI) heated plasmas. Lithium has the potential for control of this density rise due to its ability to absorb the atomic and ionic deuterium eflux through formation of lithium deuteride and lithiated compounds [14], which sequesters deuterium, making it unavailable for recycling. Due to the range of deuterium in lithium, and the immobility of the lithium deuteride formed in solid lithium, the absorption can saturate in the near surface layer [15], limiting the deuterium pumping capability of solid lithium. Subsequent recoating can replenish the surface with fresh lithium. Liquid lithium on the other hand has a much higher capacity for sequestering deuterium [16] because lithium-deuteride is more mobile in liquid lithium. In addition, it has potential for reactor applications [1-4]. Motivated by the long range potential

* *hkugel@pppl.gov.*

of lithium PFCs, NSTX has been investigating lithium pellet injection and lithium evaporation for density and impurity control as part of a phased, three-part approach to lithium PFCs: first (i) lithium pellet injection [5], then (ii) lithium evaporators [6-8] and recently lithium powder [8], and finally (iii) a liquid lithium divertor [17, 18]. This staged approach is allowing NSTX control systems, diagnostics, and research to be adapted to the evolving lithium technology.

## 2. Thin Solid lithium Coatings on Graphite

In NSTX, the range of the 500-2000eV deuterium efflux incident on lithium, is 100-250 nm [15]. This restricts pumping via the formation of lithium deuteride to a relatively thin surface region that can be quickly saturated by incident ion and neutral deuterium flux. This depletes the uncombined lithium available for lithium deutride formation. Also, lithium interactions with the NSTX residual vacuum constituents ($H_2O$, CO, and $CO_2$ ) yield surface accumulations of LiOH, $Li_2O$, and $Li_2CO_3$. which further decrease the amount of lithium available for deuteride formation. In addition, lithium can diffuse into relatively pure graphite and become unavailable at the surface for lithium deuteride formation [19]. In NSTX, the diffusion of lithium was measured for the mature ATJ graphite divertor tiles to be limited to a few microns [19].

### *2.1 Thin Solid lithium Coatings in Limiter and Divertor Experiments*

TFTR obtained reduced recycling and significantly enhanced fusion performance in its "supershot" regime by starting with a thoroughly degassed inner toroidal limiter, and applying lithium deposition techniques directly into low density plasmas prior to NBI [20]. TFTR also demonstrated that lithium deposition would not yield a performance enhancement without thorough limiter degassing beforehand. Since then, Lithium Pellet Injection (LPI) was applied directly into normally fueled, diverted C-MOD, DIII-D, TdeV, and NSTX plasmas involving a variety of heating methods, but without thorough wall degassing, and confirmed that no performance improvement occurred other than a small decrease in core impurities.

#### *2.1.1 NSTX LPI with Degassed PFCs*

NSTX LPI experiments with thoroughly degassed graphite surfaces obtained a reduction in recycling, and made contact with the TFTR performance enhancement results following lithium deposition on thoroughly degassed plasma wetted surfaces. The NSTX Center Stack provides an inner toroidal limiter during plasma startup and for toroidally limited plasmas. Ohmic helium, Center Stack Limited (CSL) discharges, and Lower Single Null (LSN) diverted conditioning discharges were used to degas the Center Stack and the lower divertor. Fig.1a shows how the Dα luminosity

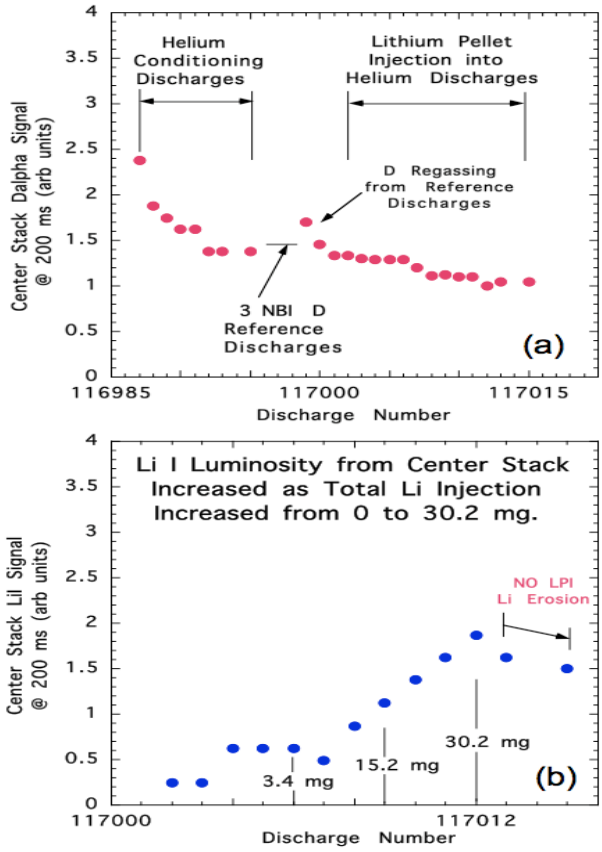


Fig.1. (a) Dα luminosity from the Center Stack region decreased during the helium conditioning as the discharge number increased, and (b) the lithium I luminosity increased.

indicates that most of the degassing had been completed, but that it continued to decrease at a much lower rate, possibly due, in part, to mild recycling from distant main chamber surfaces. Three NBI reference discharges were then applied to test the conditioning of the limiting surface which was found to be satisfactory for LPI to begin. Then, LPI was started by using 12 helium ohmic discharges, 9 with injection of either 1.7, 3.4, or 5.0 mg pellets at velocities of about 80-120 m/s. A lower rate of decrease in residual Dα luminosity continued during this LPI deposition sequence into helium discharges. Fig.1b shows how the Li I luminosity from the Center Stack increased as total lithium injection increased to 30.2 mg. After completion of this LPI sequence, which deposited lithium on the Center Stack, deuterium reference discharges were taken to test for a reduction in recycling. Fig.2 shows a 2 mg lithium pellet injected at 120 m/s into an helium ohmic discharge. At discharge

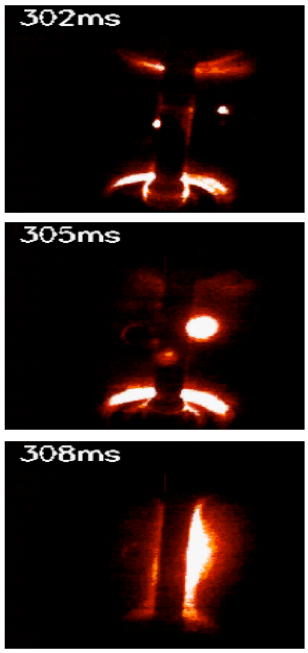


Fig.2. Plasma TV photo of a 2 mg lithium pellet injected into a He ohmic discharge. At discharge time 302 ms, it enters the plasma and proceeds toward the Center Stack. At 305ms, the lithium plasmoid the lithium plasmoid is midway toward the Center Stack, and at 308 ms, it collides.

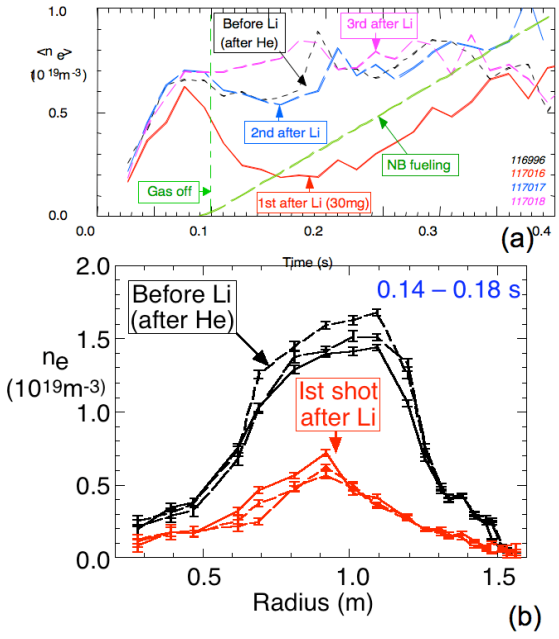


Fig.3. (a) Waveforms for first CSL D discharge following this lithium deposition sequence, and (b) the change in density profile after LPI.

time 302 ms, it enters the plasma and proceeds toward the Center Stack. At 305 ms, the lithium plasmoid is midway toward the Center Stack, and at 308 ms, it collides with it. Fig.3a shows for the first discharge following this lithium deposition sequence, the density decrease that occurred as a result of the decrease in recycling. The pumping effect of the deposited lithium decreased with the subsequent discharge and disappeared by the 3rd discharge. Fig.3b shows the change in density profile after LPI. Similar results were obtained following degassing of the lower divertor surface using diverted helium ohmic discharges followed by LPI. Fig.3a illustrates the need for a thorough degassing of graphite plasma wetted surfaces when using thin lithium coatings. These results demonstrated the effectiveness of lithium edge pumping. Subsequently, the benefits of maintaining this edge pumping capability beyond 2-3 normal discharges motivated the development of an evaporation method for investigating the characteristics of thick solid lithium coatings.

## 3. Thick Solid lithium Coatings on Graphite

As in the case of thin solid coatings, the deuterium ion and neutral pumping capacity of thick solid lithium coatings is still limited by the 100-250 nm range of deuterium efflux in lithium [15]. However, thicker coating applications, depending on the application technique can provide more pumping capacity by allowing for thicker depositions in far chamber regions not reached with thin coating techniques. In addition, in laboratory experiments thick coatings on stainless steel substrates have been found to be able saturate reactions with surface impurities, thereby allowing subsequently deposited lithium ions to provide an active lithium coating.

### *3.1 NSTX lithium Evaporation Techniques*

NSTX has been applying thick solid lithium coatings to the lower divertor region since 2007. In 2009, about 80% of the experiments used these coatings. Fig.4a shows a schematic diagram of one of two identical lithium EvaporatoR (LITER) units, used to apply these coatings. The liquid lithium capacity of each oven is 90 g. The main probe and oven axis are inclined 22° from the vertical to allow passage through the NSTX upper divertor ports. The oven output aperture is inclined an additional 10° downward from the probe drive axis so as to aim at the inner lower divertor region. The stainless steel (304-SS) oven is clad with resistive wire heaters. The output aperture has a separate heater that is operated at a higher temperature than the main oven so as to prevent lithium condensate build up. The heaters are clad with alumina-based, ceramic cloth covered by an outer 304-SS radiation shield. The LITER oven temperatures

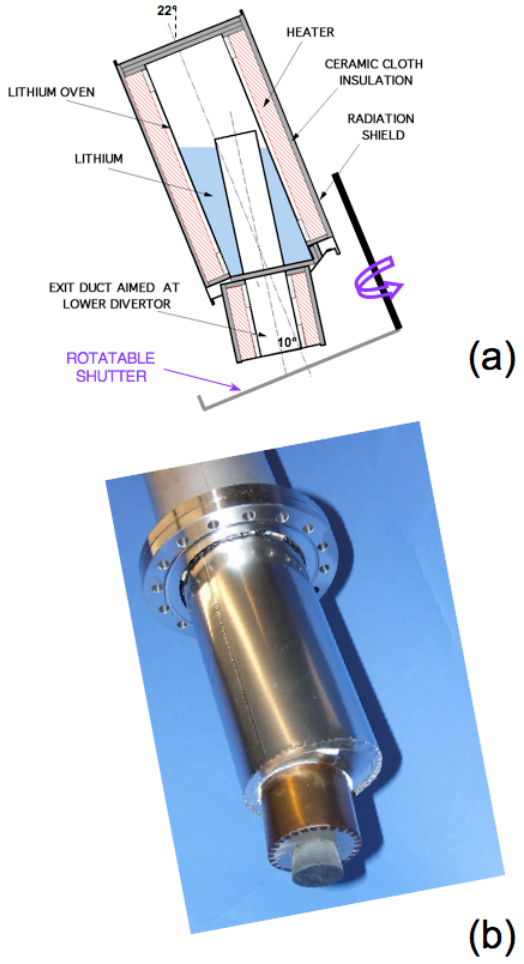


Fig.4 (a) Shows a schematic diagram of the lithium EVaporatoR (LITER), and (b) shows a photograph of the unit loaded with lithium under argon and sealed with a rubber stopper which is removed prior to installation.

which close, and interrupt the lithium vapor streams, when the diagnostic window shutters are open during a discharge. Fig. 4b shows a photograph of the oven mounted on the insertion probe. Fig.5 shows a schematic diagram of the poloidal cross section of NSTX, and the locations of two LITERs at toroidal angles 165° and 315°, and the LITER central axes aimed at the lower divertor. The shaded regions indicate the measured half-angle of the roughly Gaussian measured angular distribution at the 1/e intensity. Fig.6a illustrates the timing sequence for LITER deposition prior to the installation of the shutters. The machine discharge repetition time was about every 15 min. Helium glow-discharge cleaning (HeGDC) was applied between discharges for up to 6.5 min as required by the experiment in progress. Due to the thermal inertia of the LITER units, they were unable to cool down during this short time, and hence, they were operated to

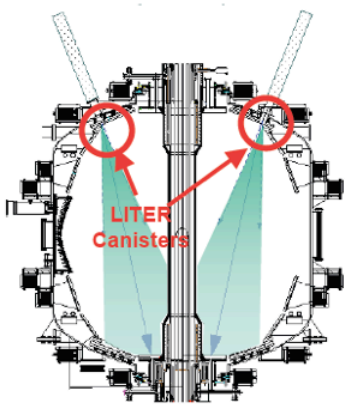


Fig.5. (a) Schematic diagram of the poloidal cross section of NSTX, and (b) the locations of two LITERS at toroidal angles 165° and 315°, and the LITER central axes aimed at the lower divertor. The shaded regions indicate the measured gaussian half-angle at the 1/e intensity of the measured evaporated lithium angular distributions.

continuously evaporate during this between discharges. Since 2008, the evaporators have been equipped with shutters, also shown also in Fig.4a, in front of the output aperture between-discharge time so as to maintain the same discharge rate per day. The disadvantages of this approach were two-fold. First the diagnostic windows received some “off target” lithium deposition during the discharge, and secondly, the HeGDC caused lithium to ionize and to be codeposited with helium incident on the PFC surface. This trapped helium which slowly diffused out on a time-scale of 10s of minutes and resulted in

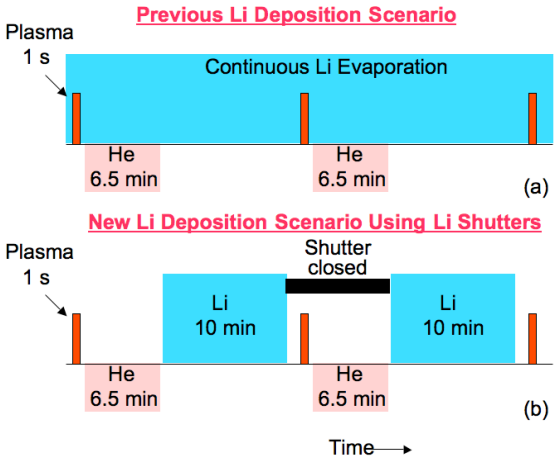


Fig.6. (a) Timing sequence for LITER deposition prior to the installation of the shutters, and (b) the respective lithium shutters closed.

helium dilution of the subsequent deuterium plasma. Fig. 6b illustrates the present lithium deposition scenario using lithium shutters. During each discharge, the LITER units are parked at the outer wall with their shutters closed. Then, if desired for the experiment in progress, HeGDC is applied for 2-6.5 min. After HeGDC is completed, the lithium shutters on the LITER units are opened, and the units are reinserted from the outer wall to their operating positions near the major radius of the graphite PFCs for the evaporation. About 30 sec before the next discharge, the LITER probes are withdrawn to their parked position and their lithium shutters are closed. This sequence is repeated automatically under computer control for each discharge during the operating day. Fig.7 shows how the signals of the lower Quartz Deposition Monitor (QDM) in direct line of sight of LITER, and that of the upper QDM not in direct line of sight of LITER increase as the total evaporated lithium increases. The variations in the lower QDM signal between discharges may be due to structural instability of thick lithium coatings on the QDM crystal. The increase in the signal of the upper QDM may be due to the transport of eroded lithium by the plasma.

### *3.2 NSTX Results Following Application of Thick Solid lithium Coatings*

NSTX thick solid lithium coatings have been applied to both well-conditioned, relatively oxygen-free, degassed divertor graphite PFCs, and also to relatively

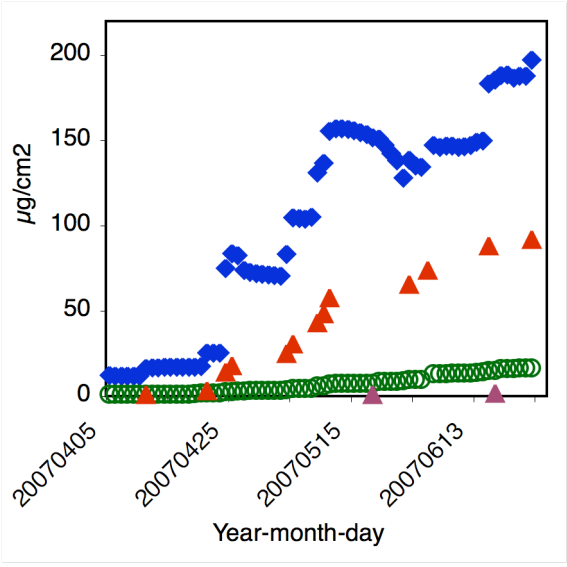


Fig.7. The signals of the lower Quartz Deposition Monitor (QDM), in direct line of sight of LITER (blue), and the upper QDM, not in direct line of sight of LITER (green, offset by 20 $\mu g/cm^2$) increase as the total evaporated Li increases (red). Dates of 10 g boronization are also shown by triangles.

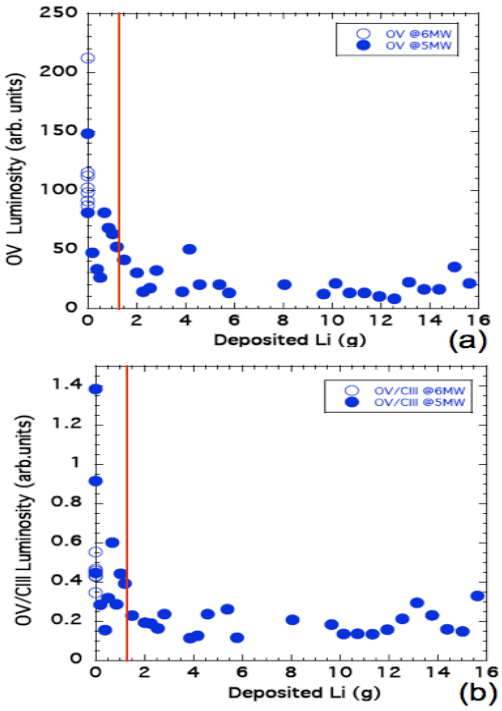


Fig.8. (a) O V and (b) OV/CIII luminosities decreased as lithium deposition increased. The vertical red line indicates the lithium deposition yielding a thickness comparable to the 250 nm range of D in lithium.

unconditioned divertor graphite PFCs exhibiting high oxygen desorption. The well-conditioned, low oxygen conditions were achieved by first removing oxides, as much as possible, from the PFCs prior to evacuation (discussed in Sec. 5 below) and after evacuation by bakeout of the PFCs at 350°C for 2 weeks, followed by deuterated trimethyboron (TMB) boronization, and 6 hours of HeGDC [7]. In the case of the application of thick lithium coatings to unconditioned divertor graphite PFCs exhibiting high oxygen desorption, the impurity gettering effect of these coatings was found to accelerate the recovery of good lithium wall conditions. Fig.8 shows for relatively unconditioned divertor graphite PFCs exhibiting high oxygen desorption, how the (a) OV luminosity, and (b) OV/CIII ratio in D plasmas decreased as lithium deposition on the lower divertor increased. At ~1.3 g total lithium deposition, average lithium deposition thickness over lower 25% of vessel becomes comparable to the 250 nm range of incident D, and the OV and OV/CIII luminosities stop decreasing. Thereafter, the relatively constant OV and OV/CIII ratios as lithium deposition over lower divertor increased may be due to oxygen contributions from the main chamber regions of partially coated graphite (e.g., upper and outer vessel hardware). Fig.9 shows how the deuterium discharge

performance responded quickly to the transition to lithium wall conditions. Fig. 10 shows waveforms exhibiting how for relatively oxygen-free pre lithium wall conditions, a thick solid lithium coating reduces deuterium recycling, suppresses ELMs [9, 21], increases stored energy, and improves confinement. Note, however, that with improved confinement and without

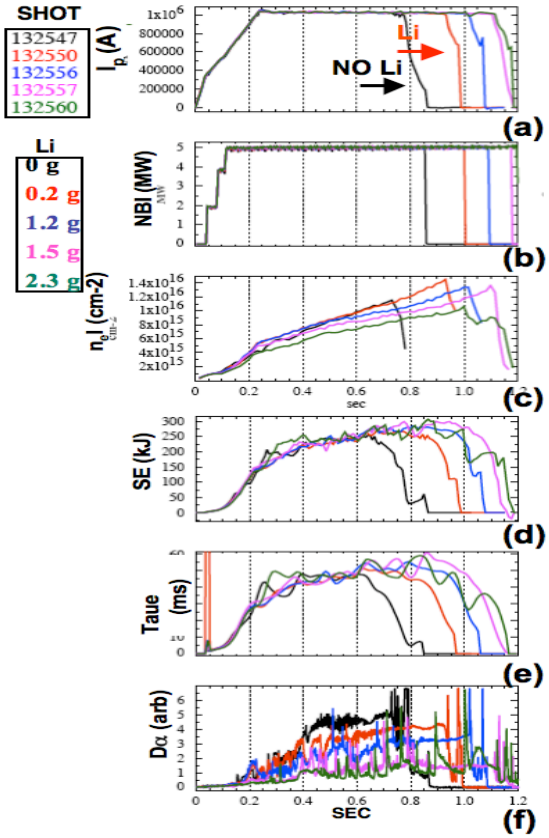


Fig.9. Starting from poor wall conditions with relatively large oxygen content, deuterium discharge performance responded quickly as the lithium coating thickness increased and NSTX transitioned to lithium wall conditions.

ELMs, impurity accumulation increases radiated power and $Z_{eff}$. In regard to impurity accumulation, quantitative measurements described below (Fig. 13) of $C^{6+}$, $Li^{3+}$ with charge-exchange recombination spectroscopy indicate that the core carbon to lithium density ratio is 30 – 100. One method to eliminate this impurity accumulation is to introduce controlled ELMs via application of 3D fields [22]. Fig. 11 shows radial profiles before (blue) and after 260 mg lithium deposition (red) at the time referenced by the vertical line in Fig.10 (0.72 s) for relatively oxygen-free pre lithium wall condition. The radial density and temperature profiles show that the transition to lithium wall conditions produced lower edge collisionality and higher edge temperatures. Fig. 12 shows a database of electron stored energy ($W_e$) *versus* total stored energy ($W_{MHD}$) for D reference plasmas immediately following lithium deposition, and for D reference plasmas prior to lithium deposition. The increase in stored energy is mostly in the electron channel. Fig. 13 shows that lithium concentration in plasmas remains low but carbon concentration rises with lithium coating. The profiles early in the discharge for both carbon and lithium are hollow but fill in as the discharge progresses. Core lithium levels are about 0.1%, whereas, the core C levels are of order 3% of the core density.

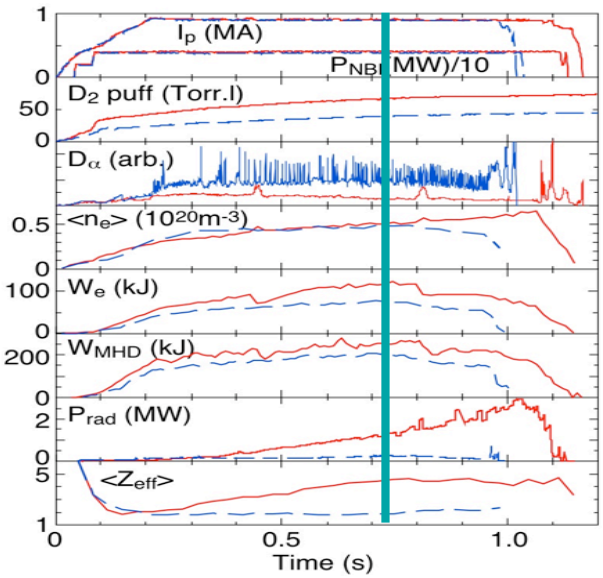


Fig.10. Reference waveforms for relatively oxygen free pre lithium wall conditions (black). After 260mg lithium deposition (red) deuterium recycling reduced, elms suppressed, stored energy increased, confinement improves. Refer to Fig.11.

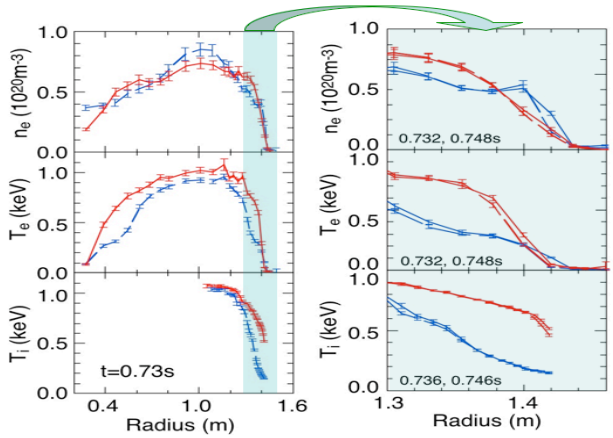


Fig.11. Radial profiles before (blue) and after 260 mg lithium deposition (red) at the time referenced by the vertical line in Fig.10 at 0.72 s for relatively oxygen free pre lithium wall condition.

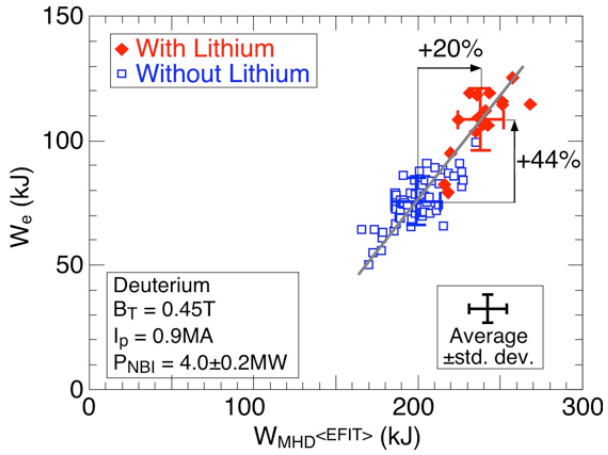


Fig.12. Electron stored energy (kJ) versus total stored energy as determined from EFIT02 (an equilibrium analysis constrained by external magnetics, electron profile shape, and diamagnetic flux).

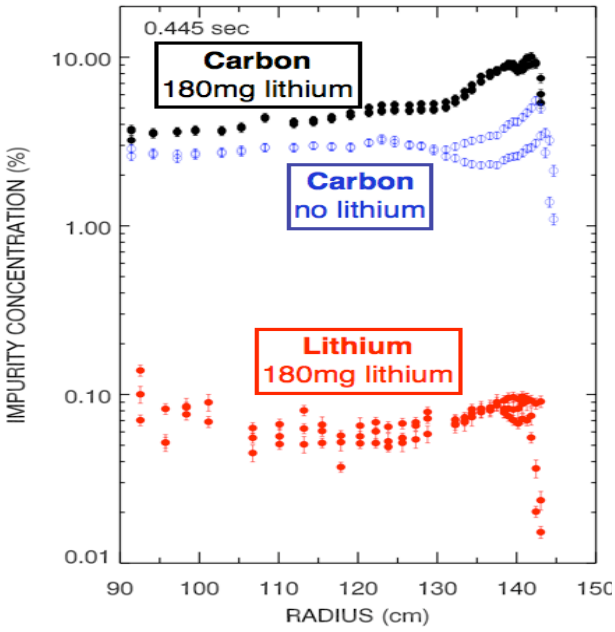


Fig.13. The results of charge exchange recombination measurements for thick lithium coatings show that absolute lithium concentration in plasmas remains low but carbon concentration rises with lithium coating.

Fig.14 shows how the broader $T_e$ profiles with lithium coating reduce both inductive and resistive poloidal flux consumption. This is a critical issue for development of low-aspect ratio tokamaks. This reduction occurs despite an increase in $<Z_{eff}>$ in ELM-free H-modes after lithium coating. An additional operating benefit, namely an increased number of discharges per day results from the gradual reduction,
and elimination of HeGDC between discharges that becomes possible as the lithium coating becomes thicker. These results demonstrated the effectiveness of lithium edge pumping. However, while the plasma performance benefits that accrued from the deposition of thick solid lithium coatings, and extended the initial results obtained with thin solid coatings, the resultant higher stored energies, hotter edge temperatures, and longer pulse lengths have not allowed the edge pumping effectiveness to be maintained without constant between-discharge evaporation to maintain stable lithium PFC conditions. The benefits of maintaining this lithium edge pumping capability for increasingly longer pulse higher power discharges has motivated work towards extending this capability.

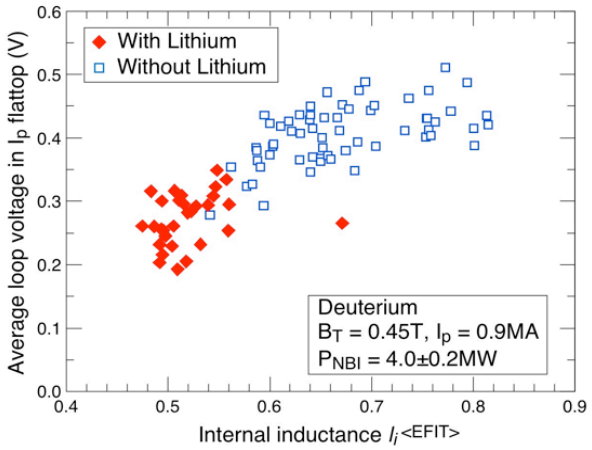


Fig.14. Average loop voltage versus internal inductance of discharges prior to lithium coating (blue) and after lithium coating (red).

**4. Liquid lithium Divertor**

The next phase of NSTX lithium work is to extend the results obtained with thick solid lithium coatings using a Liquid Lithium Divertor (LLD-1). The LLD-1 physics design goals are to achieve increased neutral beam current drive by maintaining the density at or below $n_e \sim 5 \times 10^{19}$ $m^{-3}$ at $I_p$ = 700 kA. This represents about a 15-25% decrease in density from present experiments. Key design features of the LLD-1 include providing a surface allowing liquid lithium to flow across it (wetting capability), sufficient surface area for surface tension to hold thin liquid lithium films in presence of JxB forces, and minimal temperature rate of rise of the

lithium plasma facing surface via rapid heat transfer from lithium to the copper base.

### *4.1 Liquid lithium Divertor Geometry*

In the work described above, the LITER evaporators were used to provide thick solid lithium coatings over a broad region of the lower divertor graphite PFCs. Operation with LLD-1 will change the experimental geometry by replacing a 20 cm wide toroidal conic section of outer divertor graphite PFCs with heated porous molybdenum plates [17, 18]. Fig.15 shows a recent photo of LLD-1 installed near the inner edge of the outer divertor. It consists of four 80° sections, each 20 cm wide in the radial direction. The plasma facing surface is a thin layer of 0.165 mm molybdenum plasma-sprayed with a 45% porosity on to a 0.25 mm stainless steel "skin", brazed to a 1.9 cm copper baseplate. Each toroidal section is fastened at its corners to the divertor copper baseplate with fasteners providing structural support, and electrical isolation, and allowing thermal expansion. Each toroidal section is electrically grounded to vessel at one mid-segment location to control eddy currents. Electrical heaters and gas cooling lines will be used to maintain a temperature in the range 200-400 °C. Each section is separated by graphite tiles containing at various locations magnetic sensors, thermocouples, Langmuir probes, and bias electrodes. Initially, LLD-1 and the lower divertor graphite PFCs will be lithium coated using the LITER units. Later LLD embodiments may involve a flowing lithium fill system. High-triangularity diverted discharges with the outer

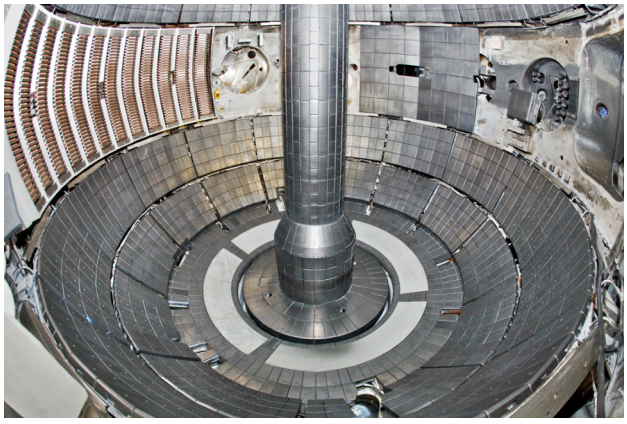

Fig.15. Photo of Liquid lithium Divertor (LLD-1) installed 2010 near the inner edge of the outer divertor, It consists of four 80° sections, each 20 cm wide in the radial direction. Each section is separated by a row of graphite diagnostic tiles containing magnetic sensors, thermocouples, Langmuir probes and bias electrodes.

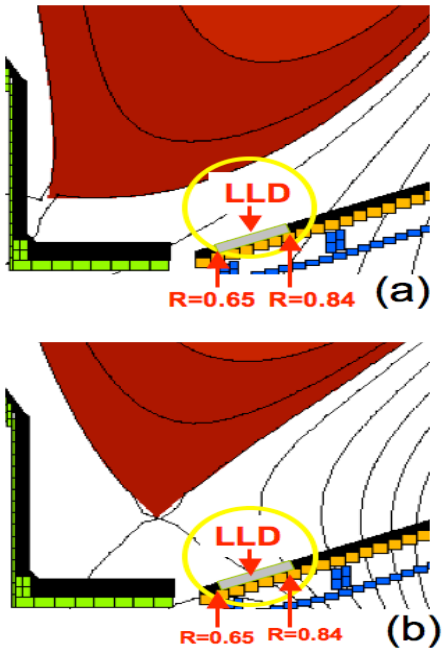


Fig.16. (a) High triangularity lower single null diverted plasma with strike point on inner divertor and open field lines incident on the LLD, and (b) medium triangularity of the plasma with most of its deuterium efflux onto the LLD.

strike point incident inboard of the LLD-1 will be pumped, via power flowing along open field lines incident on LLD-1. This is due to the high flux expansion factor (x15-20) in NSTX between the midplane and divertor (Fig.16a). Medium triangularity diverted discharges with the outer strike point incident directly on LLD-1 will be pumped through absorption (Fig.16b). The capability to apply this range of diverted discharge topologies will allow tests of the potential benefits of liquid lithium divertor for integrating high plasma and PSI performance. In particular, this will test flexible broad area pumping to reduce density for increased neutral beam current drive capability.

## 5. PFC Maintenance After Extensive lithium Operation

Since the first lihium experiments in 2005, annual NSTX lithium usage has increased until in 2009 it reached about 600 g and was employed in over 80% of the experimentally specified discharges. Under NSTX vacuum conditions, with a base pressures in the range of about $3\text{-}5\times10^{-8}$ torr, this annual lithium deposition reacts with the residual vacuum constituents ($H_2O$, CO, $CO_2$) to form lithium compounds containing oxygen, predominantly LiOH, and to a lesser extent $Li_2O$ and

$Li_2CO_3$ [14]. After an annual 12-18 week experimental campaign, NSTX is vented with the local atmosphere, and purged with humidified air for at least 1 week prior to the first personnel entry. This procedure converts any residual active lithium and LiOH to mostly $Li_2CO_3$. The vessel is then entered by a team of 3 to perform inspection, sample collection and photography. Fig.17

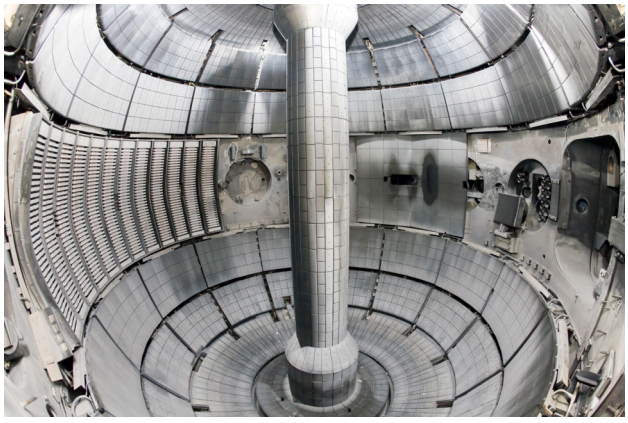

Fig.17 Wide angle photograph of NSTX after venting following 2009 experimental campaign showing the extensive white coating of lithium carbonate on all surfaces.

shows a wide angle photograph of the interior of NSTX after venting and prior to personnel entering the vessel. The white coating on all surfaces is lithium carbonate ($Li_2CO_3$). After the initial inspection work is completed, all interior surfaces are washed with deionized water and wet lint-free cloths. All graphite tiles are then sanded with Scotchbrite (an abrasive material) to remove $Li_2CO_3$ and oxides. All other metal surfaces are washed with a 5% solution of acetic acid ($CH_3COOH$ in common vinegar) to convert hard ceramic $Li_2CO_3$ to water soluble lithium acetate ($LiC_2H_3O_2$) and removal with wet lint-free cloths.The goal of these PFC cleanup procedures is to remove the oxygen bound in lithium compounds. This is very important because if, for example, all 600 g of lithium coating were converted $Li_2CO_3$, this lithium binds about 2 kg of oxygen in the form of a hard, white, nonconducting ceramic coating on all plasma facing surfaces. This oxygen if not removed is eroded by plasma interactions, and results in short, highly-radiative, high impurity content discharges.

## 6. Discussion and Conclusions

More than a decade of research has pointed to the merits and reactor relevance of replenishable liquid lithium walls for providing a pumping, impurity flushing, low-Z, self-healing plasma facing surface [1-3], and enabling a lithium wall fusion regime [4]. NSTX lithium experiments are the first extension of this work to high beta, high power, long pulse, NBI conditions in a spherical torus with divertor P/R ratios of 28-56 MW/m and eventually higher. This work has been pursued in a measured manner, allowing NSTX control systems, diagnostics, and research to be adapted to the lithium PFC conditions. NSTX experiments with LPI, evaporated lithium coatings, and lithium powder have found that relatively thin lithium coatings increased the plasma current pulse length relative to the before-lithium reference discharges, caused earlier H-mode transitions, caused significant density reduction in the early part of discharges calling for more fueling, increased electron temperature, electron stored energy and confinement time, and reduced OV/CIII impurity ratios. As the solid lithium coating thickness increases, high elongation H-mode discharges became ELM-free. Eventually the HeGDC previously routinely employed between plasma shots, was eliminated, allowing an increased duty cycle.

Characterization of the plasma performance regime achieved with the Liquid Lithium Divertor for diverted discharge topologies ranging from high to medium triangularity discharges will allow tests of the potential benefits of liquid lithium divertors for integrating high plasma and plasma surface interaction performance, and, in particular, will test flexible broad area pumping to reduce density for increased neutral beam current drive capability. This work foresees and motivates research and development needed to obtain reactor relevant designs for high power, long pulse, liquid lithium surfaces.


## Acknowledgments

This work is supported by United States Department of Energy (US DOE) Contracts DE-AC02-09CH11466 (PPPL), DE-AC05-00OR22725 (ORNL), and those of Lawrence Livermore National Laboratory in part under Contract W-7405-Eng-48 and in part under Contract DE-AC52-07NA27344, and that of Sandia, a multi-program laboratory operated by Lockheed Martin Company, for the United States Department of Energy's National Nuclear Security Administration, under contract DE-AC04-94AL85000.


## References


[1] Fus. Eng. Design **72** 1-326 (2004). A large section of the "Special Issue on Innovative High-Power Density Concepts for Fusion Plasma Chambers" highlighted progress in this effort, and it continues as a primary focus of the "Advanced Limiter/Divertor Plasma-Facing Components (ALPS) DOE program.

[2] V.A. Evtikhin *et al.*, Plasma Phys. Control Fusion **44** (2002) 955, and references therein.

[3] S. V. Mirnov, *et al*., **390-391** (2009) 876.
[4] L. E. Zakharov, Fus. Eng. and Design, **72** (2004) 149.
[5] H. W. Kugel, *et al.*, J. Nucl. Mater. **363-365** (2007) 791.
[6] H.W. Kugel, *et al.,* Physics of Plasmas **15** (2008) 056118.
[7]. H. W. Kugel, *et al*., J. Nucl. Mater., **390-391** (2009) 1000.
[8] D. Mansfield, *et al*., J. Nucl. Mater., **390-391** (2009) 764, and in this conference.
[9] R. Maingi, et. al., Phys. Rev. Lett. **103**, 075001 (2009).
[10] R. Majeski, et al., Phys. Rev. Lett., **97** (2006) 075002.
[11] R. Kaita, et al., Physics of Plasmas, **14** (2007) 056111.
[12] ] M. Ono, *et al*., Nucl. Fusion **40,** (2000) 557.
[13] M. G. Bell, *et al.*, Plasma Phys. Control. Fus. **51**, (2009) 124056.
[14] J.P. Allain, et al., J. Nuc. Mater. **390-391**, (2009) 942.
[15] J. N. Brooks, *et al*., J. Nucl. Mater., **337-339** (2005) 1053.
[16] M. J. Baldwin, *et al*., Nucl. Fusion, **42**, (2002) 1318.
[17] H. W. Kugel, *et al.,* Fusion Eng. Des. **84** (2009) 1125.
[18] R. E. Nygren *et al*.. Fusion Eng. Des. **84** (2009) 1438.
[19] W.R.Wampler, *et al*., J. Nucl. Mater. **390-391** (2009) 1009.
[20] D. K. Mansfield, etal., Phys. Plasmas **3,** (1996) 1892.
[21] L.E. Zakharov et. Al., J. Nuc. Mater., 363-365 ((2007) 453
[22] J.M. Canik, et. al., Phys. Rev. Lett. **104**, at press (2009).

The Princeton Plasma Physics Laboratory is operated
by Princeton University under contract
with the U.S. Department of Energy.

Information Services
Princeton Plasma Physics Laboratory
P.O. Box 451
Princeton, NJ 08543

Phone: 609-243-2245
Fax: 609-243-2751
e-mail: pppl_info@pppl.gov
Internet Address: http://www.pppl.gov